JCARME
ISSN: 2228-7922
Journal of Computational and Applied Research in Mechanical Engineering
Vol. 10, No. 1, pp. 101-110
jcarme.sru.ac.ir

Cooling a hot obstacle in a rectangular enclosure by using a MHD nanofluid with variable properties

Milad Darabi Boroujeni and Ehsan Kianpour*

Department of Mechanical Engineering, Faculty of Engineering, Najafabad Branch, Islamic Azad University, Najafabad, Isfahan, Iran

Article info:

Type:	Research
Received:	28/09/2017
Revised:	10/01/2019
Accepted:	23/01/2019
Online:	23/01/2019

Keywords:
Numerical simulation,
Cooling,
Forced convection,
Variable properties nanofluid,
Magnetic field.

Abstract

In this study, the cooling of a hot obstacle in a rectangular cavity filled with water-CuO nanofuid is examined numerically. This cavity has an inlet and outlet, and the cold nanofluid comes from the left side of the cavity and goes out from the opposite side, after cooling the hot obstacle. All walls are insulated, and the SIMPLER algorithm is employed for solving the governing equations. The effects of fluid inertia, the magnetic field strength, the volume fraction of nanoparticles, and the place of the outlet on the heat transfer rate are scrutinized. According to the results, the average Nusselt number builds up as the outlet place goes down. In other words, when the outlet is located at the bottom of the cavity, the rate of the heat transfer is maximum. Moreover, by increasing the Reynolds number and volume fraction of nanoparticles, the average Nusselt number builds up as well.

1. Introduction

As far as conventional fluids have low thermal conductivity, they have limited the heat transfer rate in industry. Therefore, for enhancing the heat transfer, using nanofluid, dilute suspensions of nanoparticles in liquids, can be introduced as a practical approach. Quite a few studies have been conducted and devoted to extract empirical models for nanofluids and using these models in practical examples in nature and industry. Besides, introducing some applications of nanofluids in cooling systems is a recent and hot research topic that attracted the attention of different researchers [1-8]. Aghaei et al. [2] considered a trapezoidal enclosure and by employing the the finite volume method, they scrutinized the velocity field and temperature distribution in such enclosure. The working fluid was water accompanied by Cu nanoparticles which leads to considering the magnetic field in the enclosure. They found out that volume fraction of nanoparticles has a direct effect on increasing the Nusselt number and entropy generation, whilst this behaviour is reversed for the Hartmann number; and as the Hartmann number augments, both of the aforementioned numbers will be reduced. In another numerical simulation, Abbaszadeh et al. [1] employed KKL model for CuO-water nanofluid in order to consider the effects of the brownian motions of nanoparticles. The algorithm which they used was SIMPLER with the aim of finite volume method in order to solve the set of naveir-stokes

*Corresponding author
email address: ekianpour@pmc.iaun.ac.ir

equations (for obtaining the flow field) and energy equation (for measuring the temperature field). As far as their problem geometry was a parallel plate microchannel, they considered the slip boundary condition in their walls, and magnetic field effects is reflected in their study by the Hartmann number. They demonstarted that increasing the fluid inertia force, the nanoparticles density and magnetic field effect will cause an increment in total entropy generation and the anerage Nusselt number. In another study, Ababaei et al. [9] with the goal of finding the optimum location of the impediments for enhancing the heat transfer rate inside a microchannel, employed the FVM numerical method. In their study, the working nanofluid was Al_2O_3-water whose characteristics have been obtaind by Khanafer and Vafaei's [10] model that is a variable properties model. Again, they endorsed that increasing the momentum of the nanofluid will result in the enhancment of the heat transfer inside the microchannel. Therefore, it would be benefitial if we keep the Reynolds number high enough to augment the Nusselt number. With the same reason, the total entropy generation would be increased. Very recently, Hashim et al. [11] studied the heat transfer enhancement of Al_2O_3-water inside a wavy cavity using finite element numerical method. They did partial heating from the bottom wall whilst the side wavy walls were isothermal and the top wall was insulated. They used different types of oscilations for the wavy walls to find he optimum case in terms of increasing the Nusselt number. They showed that nanoparticles caused and increase in the heat transfer rate inside the cavity.

The literature review clarifies that the problem of cooling a hot square-shaped obstacle inside an enclosure has not received considerable attention. Thus, the principle objective of the current study is to analyze the cooling of a hot obstacle numerically whilst the magnetic field effects are reflected in the enclosure. The enclosure walls are insulated and the effects of fluid inertia, magnetic field strength, volume fraction of nanoparticles, and the place of outlet on heat transfer rate have been scrutinized. The study has been conducted for Re=1-100, Ha=0-40, and $\varphi = 0-4\%$.

2. Mathematical formulation

The geometry of the enclosure is shown in Fig. 1. The cold nanofluid enters from the left side and after cooling the hot impediment, it goes out from the opposite site. All of the enclosure walls are insulated and the ratio of the length to width of the enclosure is two. The working nanofluid is MHD CuO-water nanofluid (Table 1).

The naiver-stokes equations accompanied by energy equations for laminar and forced convection of the nanofluid flow are given by:

$$\frac{\partial}{\partial x}\left(\rho_{nf} u\right) + \frac{\partial}{\partial y}\left(\rho_{nf} v\right) = 0 \tag{1}$$

$$\frac{\partial}{\partial x}(uu) + \frac{\partial}{\partial y}(vu) = \frac{1}{\rho_{nf}} \times \left[-\frac{\partial p}{\partial x} + \frac{\partial}{\partial x}\left(\mu_{nf}\frac{\partial u}{\partial x}\right) + \frac{\partial}{\partial y}\left(\mu_{nf}\frac{\partial u}{\partial y}\right) - \sigma_{nf} B_0^2 u \right] \tag{2}$$

$$\frac{\partial}{\partial x}(uv) + \frac{\partial}{\partial y}(vv) = -\frac{1}{\rho_{nf}}\frac{\partial p}{\partial y} + \frac{\partial}{\partial x}\left(\nu_{nf}\frac{\partial v}{\partial x}\right) + \frac{\partial}{\partial y}\left(\nu_{nf}\frac{\partial v}{\partial y}\right) \tag{3}$$

$$\frac{\partial}{\partial x}(uT) + \frac{\partial}{\partial y}(vT) = \frac{\partial}{\partial x}\left(\alpha_{nf}\frac{\partial T}{\partial x}\right) + \frac{\partial}{\partial y}\left(\alpha_{nf}\frac{\partial T}{\partial y}\right) \tag{4}$$

and v are representative of velocity fields in this 2D environment in x and y directions, respectively. Dynamic viscosity is μ, electrical conductivity is σ, fluid density is ρ, c_p is heat capacity at constant pressure, and k is the thermal conductivity.

The dimensionless parameters for casting the mentioned equations into the non-dimensional form are as follows:

$$(X,Y) = \frac{(x,y)}{L},\ (U,V) = \frac{(u,v)L}{\alpha_{bf}},\ \theta = \frac{T-T_c}{\Delta T},\ P = \frac{pL^2}{\rho_{nf}{\alpha_{bf}}^2} \tag{5}$$

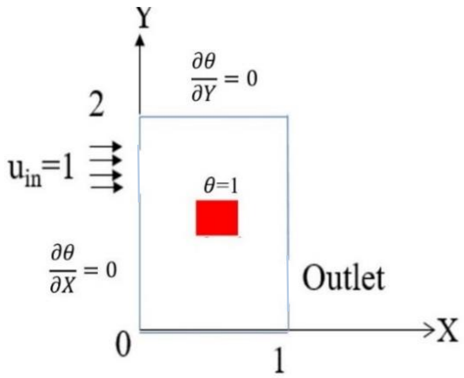

Fig. 1. Problem configuration.

Table 1. Thermo-physical properties of water as base fluid and CuO nanoparticles [12].

	ρ (kg/m^3)	c_p (J/kgK)	k (W/m K)	d_{np} (nm)	σ (Ω m)$^{-1}$
Pure water	997.1	4179	0.613	-	0.05
CuO	6500	540	18	29	10^{-10}

where $\Delta T = T_h - T_c$. Hence, the representation of the non-dimensionalized equations is:

$$\frac{\partial U}{\partial X}+\frac{\partial V}{\partial Y}=0 \tag{6}$$

$$\frac{\partial}{\partial X}(UU)+\frac{\partial}{\partial Y}(VU)=-\frac{\partial P}{\partial X}+ \frac{\rho_{bf}}{\rho_{nf}\mu_{bf}}\frac{1}{\mathrm{Re}}\left[\frac{\partial}{\partial X}\left(\mu_{nf}\frac{\partial U}{\partial X}\right)+\frac{\partial}{\partial Y}\left(\mu_{nf}\frac{\partial U}{\partial Y}\right)\right] -\frac{\sigma_{nf}}{\sigma_{bf}}\frac{\rho_{bf}}{\rho_{nf}}\frac{\mathrm{Ha}^2}{\mathrm{Re}}U \tag{7}$$

$$\frac{\partial}{\partial X}(UV)+\frac{\partial}{\partial Y}(VV)=-\frac{\partial P}{\partial Y}+ \frac{\rho_{bf}}{\rho_{nf}\mu_{bf}}\frac{1}{\mathrm{Re}}\left[\frac{\partial}{\partial X}\left(\mu_{nf}\frac{\partial V}{\partial X}\right)+\frac{\partial}{\partial Y}\left(\mu_{nf}\frac{\partial V}{\partial Y}\right)\right] \tag{8}$$

$$\frac{\partial}{\partial X}(U\theta)+\frac{\partial}{\partial Y}(V\theta)=\frac{\left(\rho c_p\right)_{bf}}{k_{bf}\left(\rho c_p\right)_{nf}}\times \frac{1}{\mathrm{RePr}}\left[\frac{\partial}{\partial X}\left(k_{nf}\frac{\partial \theta}{\partial X}\right)+\frac{\partial}{\partial Y}\left(k_{nf}\frac{\partial \theta}{\partial Y}\right)\right] \tag{9}$$

The Reynolds, Hartmann and Prandtl numbers are defined, respectively, as:

$$\mathrm{Re}=\frac{u_0 L}{\nu_{bf}};\quad \mathrm{Ha}=B_0 L\sqrt{\frac{\sigma_{bf}}{\mu_{bf}}};\quad \mathrm{Pr}=\frac{\nu_{bf}}{\alpha_{bf}} \tag{10}$$

The density, the heat capacity, the volume expansion coefficient [2] and the diffusivity coefficient of the nanofluid are calculated as:

$$\rho_{nf}=(1-\varphi)\rho_f+\varphi\rho_s \tag{11}$$

$$(\rho c_p)_{nf}=(1-\varphi)(\rho c_p)_f+\varphi(\rho c_p)_s \tag{12}$$

$$(\rho\beta)_{nf}=(1-\varphi)(\rho\beta)_f+\varphi(\rho\beta)_s \tag{13}$$

$$\alpha_{nf}=\frac{k_{nf}}{\left(\rho c_P\right)_{nf}} \tag{14}$$

In the Maxwell and Brinkman model, the viscosity [13] and thermal conductivity coefficient [14] dependent on the volume fraction of nanofluid are obtained from Eqs. (15) and (16).

$$\mu_{nf}=\mu_f(1-\varphi)^{-2.5} \tag{15}$$

$$k_{nf}=k_f\left[\frac{(k_s+2k_f)-2\varphi(k_f-k_s)}{(k_s+2k_f)+\varphi(k_f-k_s)}\right] \tag{16}$$

In Koo and Kleinstreuer model [15], the thermal conductivity coefficient and viscosity are also dependent on the temperature and the Brownian motion of nanoparticles. In this model, the thermal conductivity coefficient and viscosity are obtained from Eqs. (17) and (18), respectively. The static part of the thermal conductivity coefficient and viscosity are obtained from Eqs. (15) and (16), respectively, and the Brownian part of the thermal conductivity coefficient and viscosity are calculated from Eqs. (15-18).

$$\mu_{nf}=\mu_{static}+\mu_{Brownian} \tag{17}$$

$$k_{nf}=k_{static}+k_{Brownian} \tag{18}$$

where

$$k_{Brownian}=5\times10^4\lambda\varphi\rho_f c_{p,f}\sqrt{\frac{\kappa T}{\rho_s d_p}}\zeta\left(T,\varphi\right).\ \rho_s$$

and d_p are density and the radius of the nanoparticles, respectively. For the water-CuO nanofluid, the λ and ζ functions are estimated experimentally, and for the interval of $300<T(K)<325$,

$$\lambda = 0.0137(100\varphi)^{-0.8229} \ for \ \varphi \le 1\% \qquad (19)$$
$$\lambda = 0.0011(100\varphi)^{-0.7272} \ for \ \varphi > 1\%$$

κ is the Boltzmann constant ($\kappa = 1.3807\times10^{-23}\ J/K$). $\mu_{Brownian}$ is also obtained from the following relation:

$$\mu_{Brownian} = \frac{k_{Brownian}}{k_f} \times \frac{\mu_f}{Pr} \qquad (20)$$

The local Nusselt number is:

$$\mathrm{Nu} = -\left(\frac{k_{nf}}{k_f}\right)\frac{\partial\theta}{\partial n}\bigg|_{wall} \qquad (21)$$

where n is the normal direction from the hot obstacle. Thus, the average Nusselt number can be calculated by integrating Eq. (21) along the hot obstacle:

$$\mathrm{Nu}_{\mathrm{av}} = \frac{\int_L \mathrm{Nu}\,dL}{\int_L dL} \qquad (22)$$

3. Numerical implementation

The numerical method used in this study is called SIMPLER algorithm and Finite Volume Method (FVM). In this method, initially, a fine grid should be defined over the problem domain and around each node, a volume is considered. Then, after integrating and discretizing equations, the PDEs will be simplified. Then, with the help of line-by-line TDMA solver, the discretized equations are solved.

3.1. Grid independence test

If the results of a numerical simulation depends on the grids size, the accuracy of the results will be overshadowed. Thus, we run a grid independency test to ensure the accuracy of the results. Our test is for CuO-water nanofluid in the enclosure at Re=100 and Ha=0. The obtained average Nusselt number for different girds is presented in Table 2. It shows that 41×81 is the most suitable grid size, which ensures grid independency.

Table 2. Average Nusselt number in $\mathrm{Ha} = 40$ and $\mathrm{Re} = 10$ $\phi = 0.03$.

Grid size	$\mathrm{Nu}_{\mathrm{av}}$	Relative difference
41×21	19.14	-
81×41	16.10	13.46
161×81	16.38	1.74

3.2. Computer program verification

In order to ascertain the validity of the computer used in this study, some cases of Xu et al. [16] are modeled with the current program and their results are evaluated in Fig. 3. Also, the geometry of the Xu et al. [16] is presented in Fig. 2. In Fig. 3 the streamlines are depicted as the Lewis number changes. The plots show an excellent conformance between our simulation and those of Xu et al. [16] which ensures the accuracy of the modeling results. Also, it should be noted that the ratio of thermal diffusivity to mass diffusivity is considered as the Lewis number.

4. Results and discussion

In the present numerical study, navire-stokes and energy equations have been solved in an enclosure filled with water-CuO nanofluid. There is a hot obstacle in the middle of the enclosure and all of the walls of the enclosure are adiabatic. Different dimensionless parameters such as Re, Ha, and φ have been considered as the inputs and their influence has been monitored by calculating the Nu_{avg}. This study was conducted for Re=1-100, Ha=0-40, and $\varphi = 0-4\%$.

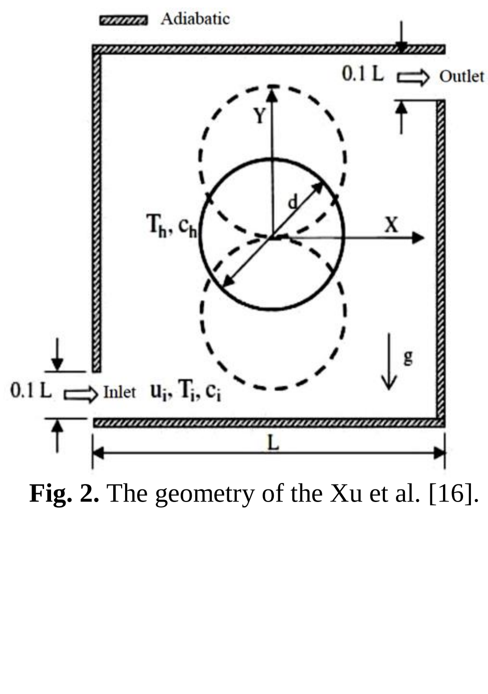

Fig. 2. The geometry of the Xu et al. [16].

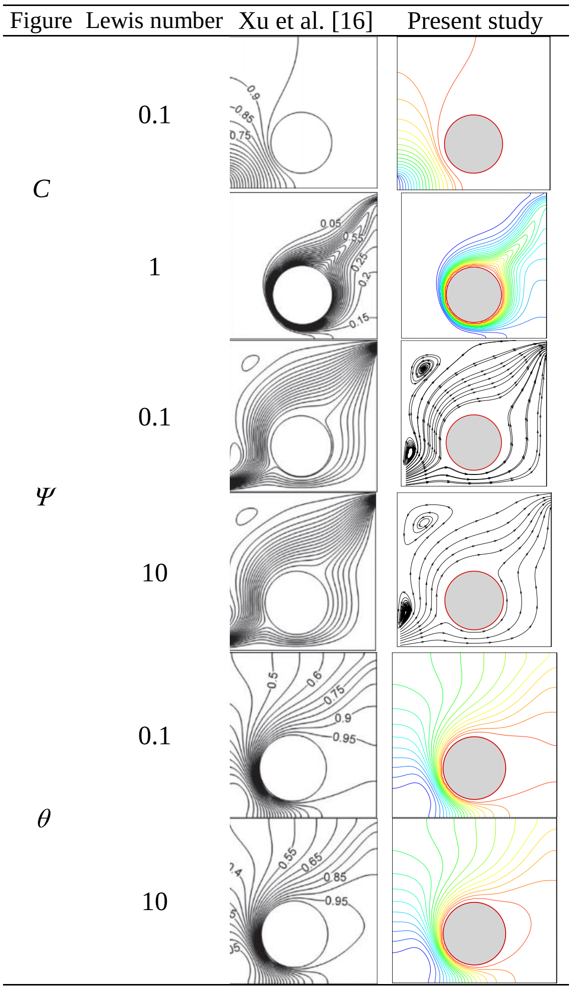

Fig. 3. Comparisons of the present study and the study of Xu et al [16].

4.1. The effects of the outlet place

Streamlines and isothermal lines versus the outlet place of the enclosure is displayed in Fig. 4 for Re=10, Ha=20, and $\varphi = 4\%$. Generally, when the outlet is at the bottom of the cavity, the streamlines are more irregular and as a result, the velocity of the nanofluid is higher. Furthermore, when the outlet is located at the top of the cavity, most of the streamlines exit from the cavity directly and the intensity of the flow in the bottom of the obstacle is low. However, when the outlet is placed at the bottom of the cavity, the flow is devided symmetrically between both sides of the hot obstacle that shows the intensity of the flow is the same at the both sides of the obstacle. Moreover, the streamlines for the nanofluid and pure fluid have no visible difference.

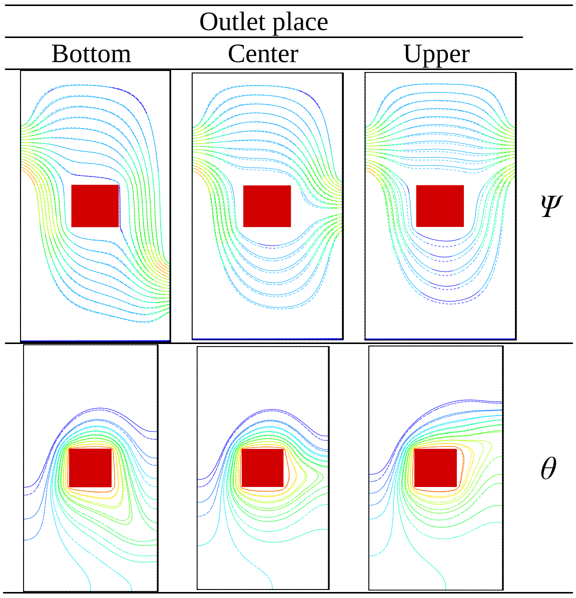

Fig. 4. Streamlines and isothermal lines versus the outlet place of the enclosure in Re=10, Ha=20, and $\varphi = 4\%$ for nanofluid (—) and pure fluid (– –).

Regarding the isothermal lines, in all cases, the isothermal lines are drawn from the hot obstacle to the outlet. Moreover, when the outlet is located at the top of the cavity, a cold region is seen at the top of the obstacle; and when the outlet goes down, the dimension of this region increases significantly and as a result, the cold lines enter around the hot obstacle. This phenomenon leads to compressing the isotherm lines over the hot obstacle and as a result, the temperature gradient through the cavity increases and finally, the rate of heat transfer augments. Furthermore, the isothermal lines for pure fluid are closer to the hot obstacle in comparison to isothermal lines for nanofluid due to the fact that the diffusity of fluid is lower than nanofluid$\left(\alpha_{bf} < \alpha_{nf}\right)$.

Fig. 5 shows the heat transfer rate on the hot surfaces of the obstacle in terms of outlet palce in Re=20, Ha=10, and $\varphi = 4\%$. As it is crystal clear from this figure, the Nu_{avg} decreases as the place of the eoutlet goes down.

In Fig. 6, the local Nusselt number variations on the upper and bottom surfaces of the hot obstacle in terms of outlet place are illustrated in Re=20, Ha=10, and $\varphi = 4\%$. . Generally, the local Nusselt number is more in the upper surface of the obstacle than the lower surface as far as the fluid, which reaches the top surface, is colder than the fluid, which reaches the lower surface; and as a result, in the top surface the heat capacity is by far more than the lower surface.

In Fig. 7, variations of the local Nusselt number on the left and right surfaces of the hot obstacle in terms of outlet place are illustrated in Re=20, Ha=10, and $\varphi = 4\%$. . Generally, the Nu_{loc} is more in the left surface of the obstacle than the right surface since the fluid that reaches the left surface is colder than the fluid that reaches the right surface; as a result, in the left surface the heat capacity is by far more than the right surface.

4.2. Streamlines and isotherm lines

Variations of the streamlines for different hartmann and Reynolds numbers in $\varphi = 4\%$ are dispalyed in Fig. 8.

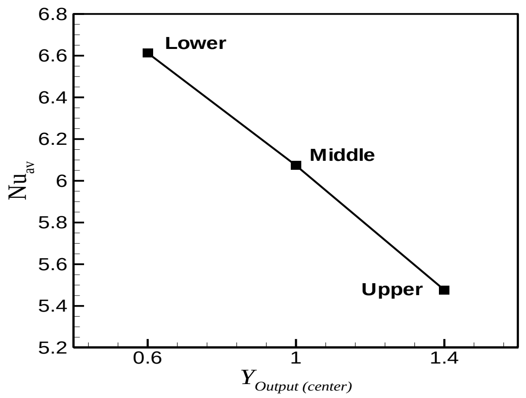

Fig. 5. Average Nusselt number variations on the hot surfaces of the obstacle in terms of outlet palce in Re=20, Ha=10, and $\varphi = 4\%$.

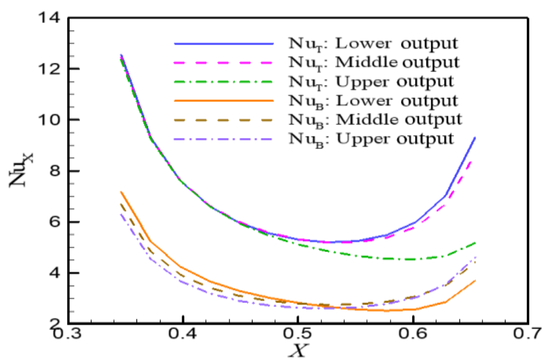

Fig. 6. Variations of the Nu_{loc} on the upper and bottom surfaces of the hot obstacle in terms of outlet place in Re=20, Ha=10, and $\varphi = 4\%$. .

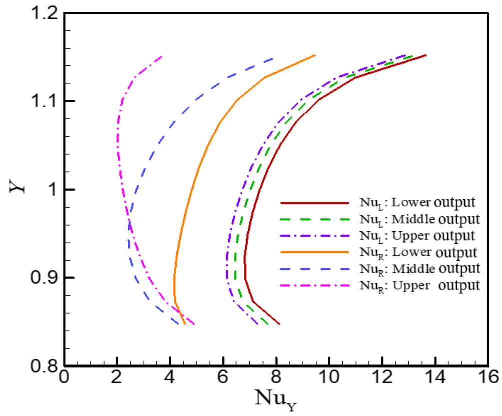

Fig. 7. Variations of the local Nusselt number on the left and right surfaces of the hot obstacle in terms of outlet place in Re=20, Ha=10, and $\varphi = 4\%$. .

In Ha=0 and when there is no magnetic field, by increasing the Reynolds number, the flow is not layered anymore and it is drawn to the outlet. In high Reynolds number, the momentum force are intensified and they overcome the viscosity forces and as a result, a second counter clockwise vortex is created at the top of the cavity; and as the Reynolds number augments, its dimension rises too. Moreover, in Hartmann numbers of 20 and 40, the variation of the Reynolds number have no visible effects on the flow and the flow is completely governed by the magnetic field since the flow becomes weaker as the Ha increases. Furthermore, by increasing the Hartmann number from 20 to 40, it is obvious that the devation of the streamlines reduces and the flow is drawn to the walls. This phenomenon occured as far as the magnetic forces have a direct but negative relationship with the velocity of thwe flow ($-\frac{Ha^2}{Re}U$). So, in regions where the horizontal velocity is more, the magnetic forces weakens the flow more and the streamlines lose their deviations.

Fig. 9. shows the variations of the isothermal lines for different hartmann and Reynolds numbers in $\varphi = 4\%$ for nanofluid and base fluid. In Re=1 and in all of the Hartmann numbers, the flow is cold near the entrance and as it makes a contact with the hot obstacle, it becomes warmer; and the isothermal lines are spreaded through the cavity; and a lower temperature gradient is seen on the hot obstacle. By increasing the Reynolds number, the isothermal

lines are more compressed and the dimension of the cold region near the entrance augments. So, the isothermal lines approaches the hot obstacle more and more as the Reynolds number augments; and as a result, the heat transfer increases. It is worth mentioning that with the augmentation of the Hartmann number, the general pattern of the isothermal lines sees no changes. Finally, it should be noted that the temperature gradient on the hot obstcale is lower for nanofluid than pure fluid.

4. 3.Velocity profile and temperature field

Variations of the dimensionless temperature relative to the horizontal location in the central section of the enclosure in different Reynolds number for Ha=20, and $\varphi = 4\%$ are shown in Fig. 10.

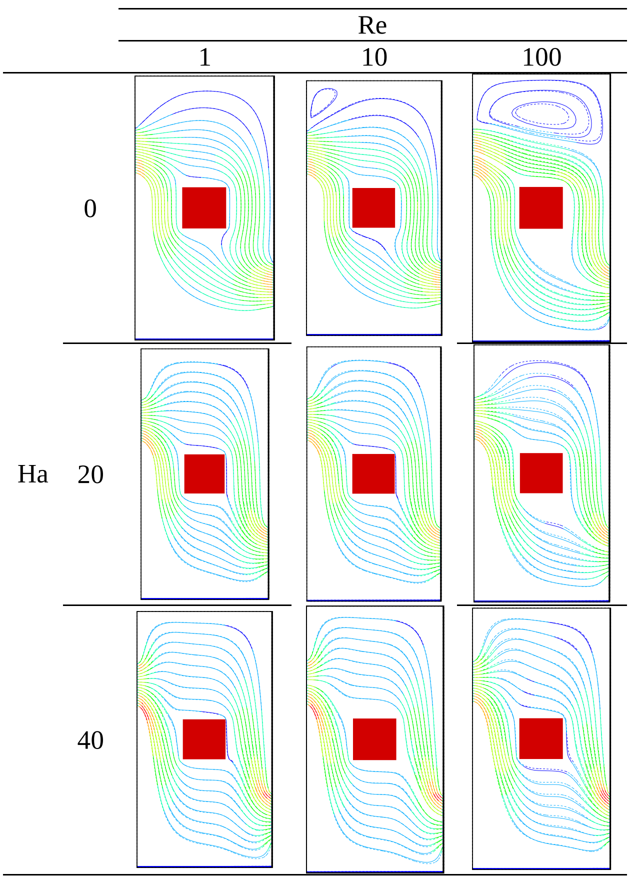

Fig. 8. Variations of the streamlines for different hartmann and Reynolds numbers in $\varphi = 4\%.$ for nanofluid(—) and pure fluid(– –).

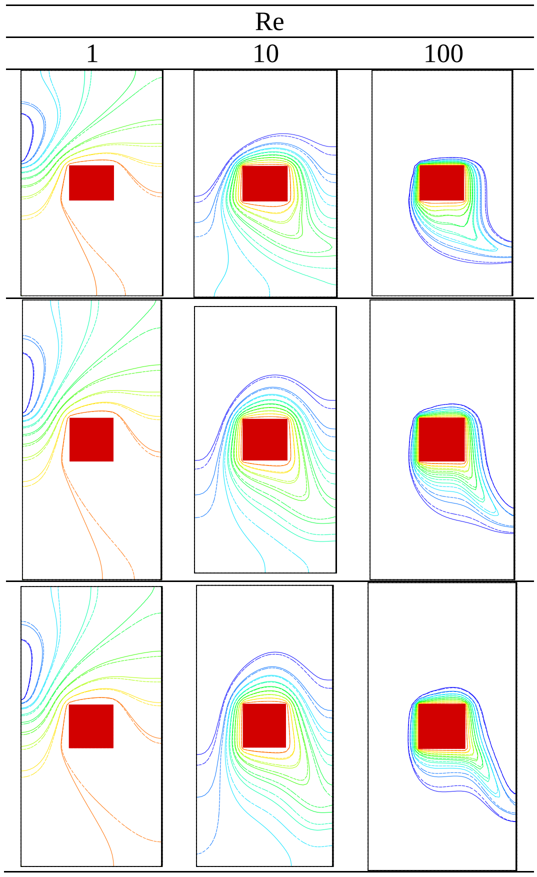

Fig. 9. Variations of the isothermal lines for different hartmann and Reynolds numbers in $\varphi = 4\%.$ for nanofluid(—) and pure fluid(– –).

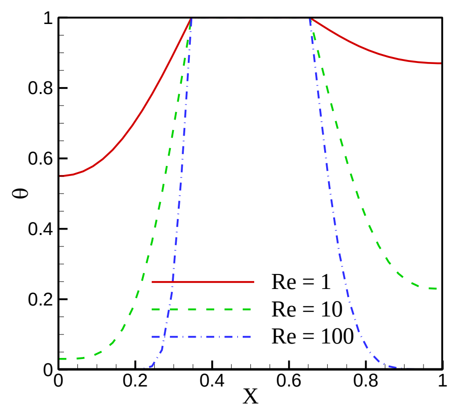

Fig. 10. Variations of the dimensionless temperature relative to the horizontal location in the central section of the enclosure in different Reynolds numbers for Ha=20, and $\varphi = 4\%$. .

According to this figure, by increasing the Reynolds number, the horizontal temperature gradient increases on the hot obstacle and as a result, the heat transfer increases. In Fig. 11 and similar to the horizontal case, the vertical temperature gradient increases on the hot obstacle and as a result, the heat transfer increases. Figs. 12 and 13, show the variations of the dimensionless velocity relative to the horizontal and vertical location in the central section of the enclosure in different Reynolds numbers for Ha=20, and $\varphi = 4\%$. .

According to these figures, by increasing the Reynolds number from 1 to 10, no changes are seen as far as the magnetic forces have control over the flow. But, when the Re=100, the flow pattern changes somehow and the momentum forces increase.

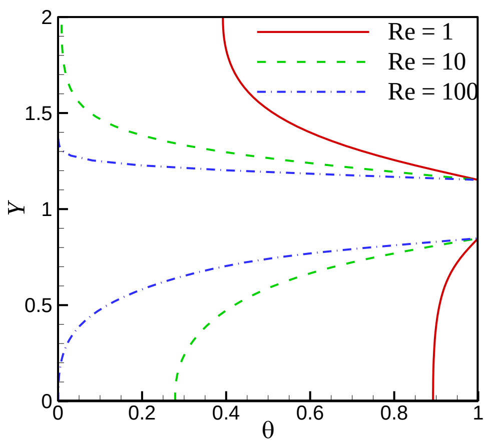

Fig. 11. Variations of the dimensionless temperature relative to the vertical location in the central section of the enclosure in different reynolds for Ha=20, and $\varphi = 4\%$.

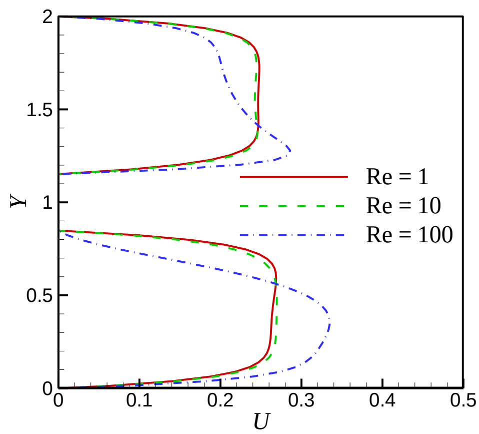

Fig. 12. Variations of the dimensionless velocity relative to the horizontal location in the central section of the enclosure in different reynolds numbers for Ha=20, and $\varphi = 4\%$.

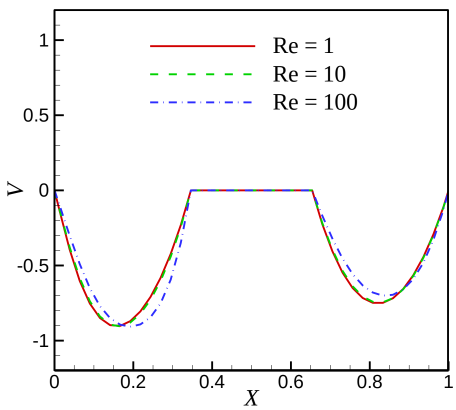

Fig. 13. Variations of the dimensionless velocity relative to the vertical location in the central section of the enclosure in different reynolds numbers for Ha=20, and $\varphi = 4\%$.

4.4. Heat transfer rate

Fig. 14. illustrates the variations of the average heat transfer rate in terms of the Reynolds number in Ha=20 and in different volume fractions of nanoparticles. According to this figure, by increasing the reynolds number, the Nusselt number and heat transfer augmentsince the tempetarure gradient increases over the hot obstacle. Also, increasing the volume fraction of nanoparticles results in the augmentation of the heat transfer. Furthermore, and based on Fig. 15. the average Nusselt number and heat transfer have an inversed relationship with the magnetic field force and increasing the hartmann number leadsf to decreasing the heat transfer.

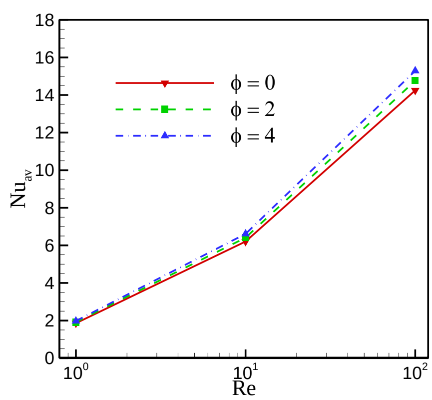

Fig. 14. Variations of the average Nusselt number in terms of Reynolds number in Ha=20 and in different volume fractions of nanoparticles.

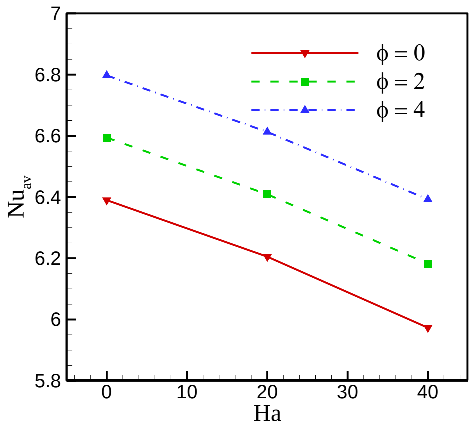

Fig. 15. Variations of the average Nusselt number in terms of Hartmann number in Re=10 and in different volume fractions of nanoparticles.

5. Conclusions

In this study, the SIMPLER algorithm and Finite Volume Method are employed to investigate the MHD effects on the flow structure and heat transfer of a water-CuO nanofluid in order to chill a hot obstacle inside a rectangular cavity. The walls of the cavity are insulated, and the effects of fluid inertia, magnetic field strength, volume fraction of nanoparticles on the heat transfer rate are investigated. The study is conducted for Re=1-100, Ha=0-40, and $\varphi = 0 - 4\%$. The results show that:

1. When the outlet is at the bottom of the cavity, the streamlines are more irregular, and as a result, the velocity of the nanofluid is more.
2. The Nu_{avg} decreases as the place of outlet goes down.
3. By increasing the Reynolds number, the horizontal temperature gradient increases on the hot obstacle, and as a result, the heat transfer increases.
4. The average Nusselt number and heat transfer have an inversed relationship with the Ha, and increasing the Ha leads to decrease the heat transfer.

References

[1] M. Abbaszadeh, A. Ababaei, A. A. A. Arani and A. A. Sharifabadi, "MHD forced convection and entropy generation of CuO-water nanofluid in a microchannel considering slip velocity and temperature jump," *Journal of the Brazilian Society of Mechanical Sciences and Engineering*, Vol. 39, No. 3, pp. 775-790, (2017).

[2] A. Aghaei, H. Khorasanizadeh, G. a. Sheikhzadeh and M. Abbaszadeh, "Numerical study of magnetic field on mixed convection and entropy generation of nanofluid in a trapezoidal enclosure," *Journal of Magnetism and Magnetic Materials*, Vol. 403, pp. 133-145, (2016).

[3] A. R. Rahmati, A. R. Roknabadi and M. Abbaszadeh, "Numerical simulation of mixed convection heat transfer of nanofluid in a double lid-driven cavity using lattice Boltzmann method," *Alexandria Engineering Journal*, Vol. 55, No. 4, pp. 3101-3114, (2016).

[4] M. Mollamahdi, M. Abbaszadeh and G. A. Sheikhzadeh, "Flow field and heat transfer in a channel with a permeable wall filled with Al2O3-Cu/water micropolar hybrid nanofluid, effects of chemical reaction and magnetic field," *Journal of Heat and Mass Transfer Research (JHMTR)*, Vol. 3, No. 2, pp. 101-114, (2016).

[5] G. Sheikhzadeh, H. Ghasemi and M. Abbaszadeh, "Investigation of natural convection boundary layer heat and mass transfer of MHD water-AL2O3 nanofluid in a porous medium," *International Journal of Nano Studies & Technology (IJNST)*, Vol. 5, No. 2, pp. 110-122, (2016).

[6] G. Sheikhzadeh, A. Aghaei, H. Ehteram and M. Abbaszadeh, "Analytical study of parameters affecting entropy generation of nanofluid turbulent flow in channel and micro-channel," *Thermal Science*, (2016).

[7] A. Abbasian Arani, J. Amani and M. Hemmat Esfeh, "Numerical simulation of mixed convection flows in a square double lid-driven cavity partially heated using nanofluid," *Journal of Nanostructures*, Vol. 2, No. 3, pp. 301-311, (2012).

[8] A. Ababaei, M. Abbaszadeh, A. Arefmanesh and A. J. J. N. H. T. Chamkha, Part A: Applications,

"Numerical simulation of double-diffusive mixed convection and entropy generation in a lid-driven trapezoidal enclosure with a heat source," pp. 1-19, (2018).

[9] A. Ababaei and M. J. G. J. o. N. Abbaszadeh, "Second Law Analyses of Forced Convection of Low-Reynolds-Number Slip Flow of Nanofluid Inside a Microchannel with Square Impediments," Vol. 1, No. 4, (2017).

[10] K. Khanafer, K. J. I. j. o. h. Vafai and M. transfer, "A critical synthesis of thermophysical characteristics of nanofluids," Vol. 54, No. 19-20, pp. 4410-4428, (2011).

[11] I. Hashim, A. Alsabery, M. Sheremet and A. J. A. P. T. Chamkha, "Numerical investigation of natural convection of Al2O3-water nanofluid in a wavy cavity with conductive inner block using Buongiorno's two-phase model," (2018).

[12] A. Arefmanesh, A. Aghaei and H. Ehteram, "Mixed convection heat transfer in a CuO–water filled trapezoidal enclosure, effects of various constant and variable properties of the nanofluid," *Applied Mathematical Modelling*, Vol. 40, No. 2, pp. 815-831, (2016).

[13] H. Brinkman, "The viscosity of concentrated suspensions and solutions," *The Journal of Chemical Physics*, Vol. 20, No. 4, pp. 571-571, (1952).

[14] J. Maxwell Garnett, "Colours in metal glasses and in metallic films, Philos. Tr. R. Soc. S.-A, 203, 385–420," ed, (1904).

[15] J. Koo and C. Kleinstreuer, "A new thermal conductivity model for nanofluids," *Journal of Nanoparticle Research*, Vol. 6, No. 6, pp. 577-588, (2004).

[16] H. Xu, Z. Wang, F. Karimi, M. Yang and Y. Zhang, "Numerical simulation of double diffusive mixed convection in an open enclosure with different cylinder locations," *International Communications in Heat and Mass Transfer*, Vol. 52, pp. 33-45, (2014).

How to cite this paper:

P. Sreenivasulu, B. Vasu, T. Poornima and N. Bhaskar Reddy, "Inclined lorentzian force effect on tangent hyperbolic radiative slip flow imbedded carbon nanotubes: lie group analysis", *Journal of Computational and Applied Research in Mechanical Engineering*, Vol. 10, No. 1, pp. 101-110, (2020).

DOI: 10.22061/jcarme.2019.2959.1308

URL: http://jcarme.sru.ac.ir/?_action=showPDF&article=991